Supplementary Information

Application of Multi-Task Learning in Analyzing the Methane Working Capacity of Metal-Organic Frameworks

Junhui Kou[a, b], Tianle Liu[a, b, *], Guosheng Jiang[a, b], Guokun Yang[a, b], Zerang Li[a, b], Xiaoyang Ni[b], Hao Liu[b]

[a] Unconventional Cementing and Special Reinforcement Laboratory, Wuhan, 430074, China

[b] Faculty of Engineering, China University of Geosciences, Wuhan, 430074, China

* Corresponding author.

E-mail address: liutianle@cug.edu.cn

S1. Descriptors

Table S1

Definition of geometric descriptors.

Descriptor	Definition	Units
UCv	Unit cell volume	$Å^3$
Density	Density of MOFs	g/cm^3
LCD	Largest cavity diameter	Å
PLD	Pore limiting diameter	Å
DFSP	Diameter of largest free sphere path	Å
AVA	Accessible volume per unit cell	$Å^3$
Vf	Volume fraction	/
Vg	Gravimetric volume	cm^3
ASA	Accessible surface area per unit cell	Å
SAv	Volumetric surface area	m^2
SAg	Gravimetric surface area	m^2/g
POAVA	Probe-occupiable volume per unit cell	$Å^3$
POVf	Probe-occupiable volume fraction	/
POVg	Probe-occupiable gravimetric volume	cm^3/g

S2. Model Architecture

After standardization, the training set was first input to the shared layers, consisting of two fully connected layers. The first layer contained 128 neurons with ReLU activation, and a dropout rate of 0.5 was applied to randomly deactivate neurons to mitigate overfitting. The output was then passed through a second fully connected layer with 64 neurons, also using ReLU activation and a dropout rate of 0.5. The output from the shared layers entered the attention layer, where input features were transformed and attention scores computed via two fully connected layers and tanh activation, producing weighted context vectors and corresponding attention weights. Finally, the context vectors were passed through task-specific output layers to generate predictions, with each task assigned an individual output layer.

S3. Model prediction performance

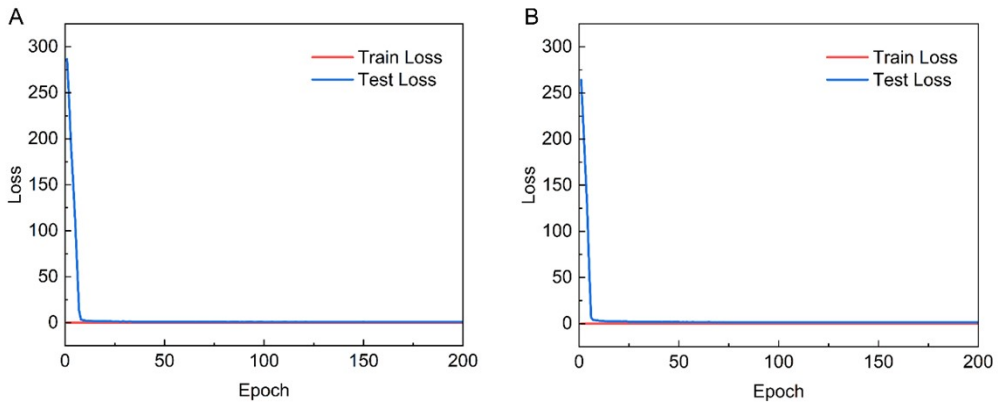

Fig. S1. Training loss curves for the models. (A) Full-feature model; (B) Feature-optimized model.

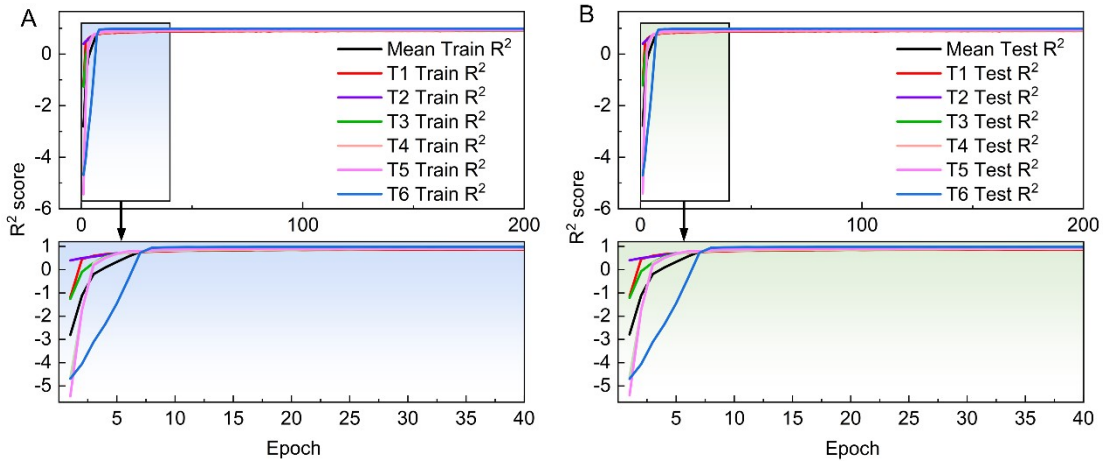

Fig. S2. R^2 training curve for the full-feature models.

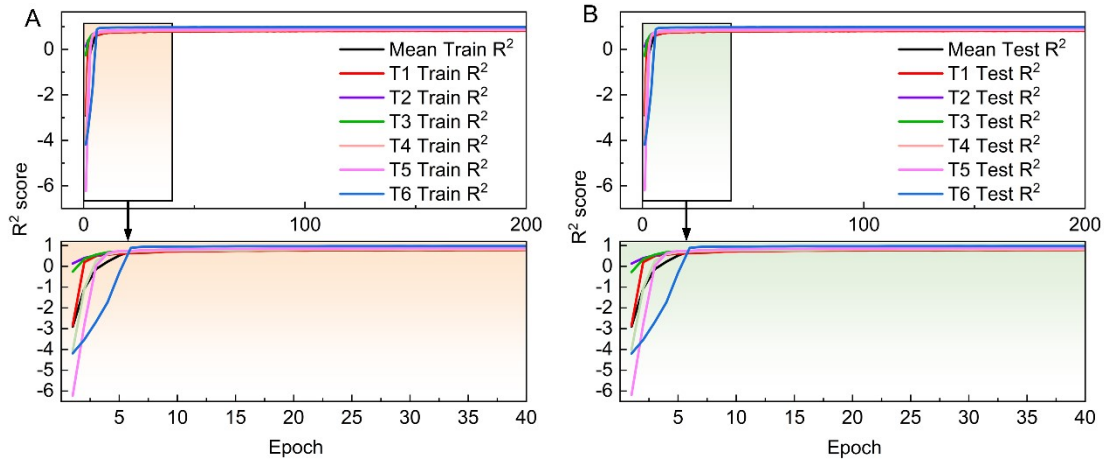

Fig. S3. R^2 training curve for the feature-optimized models.

S4. Dependency analysis

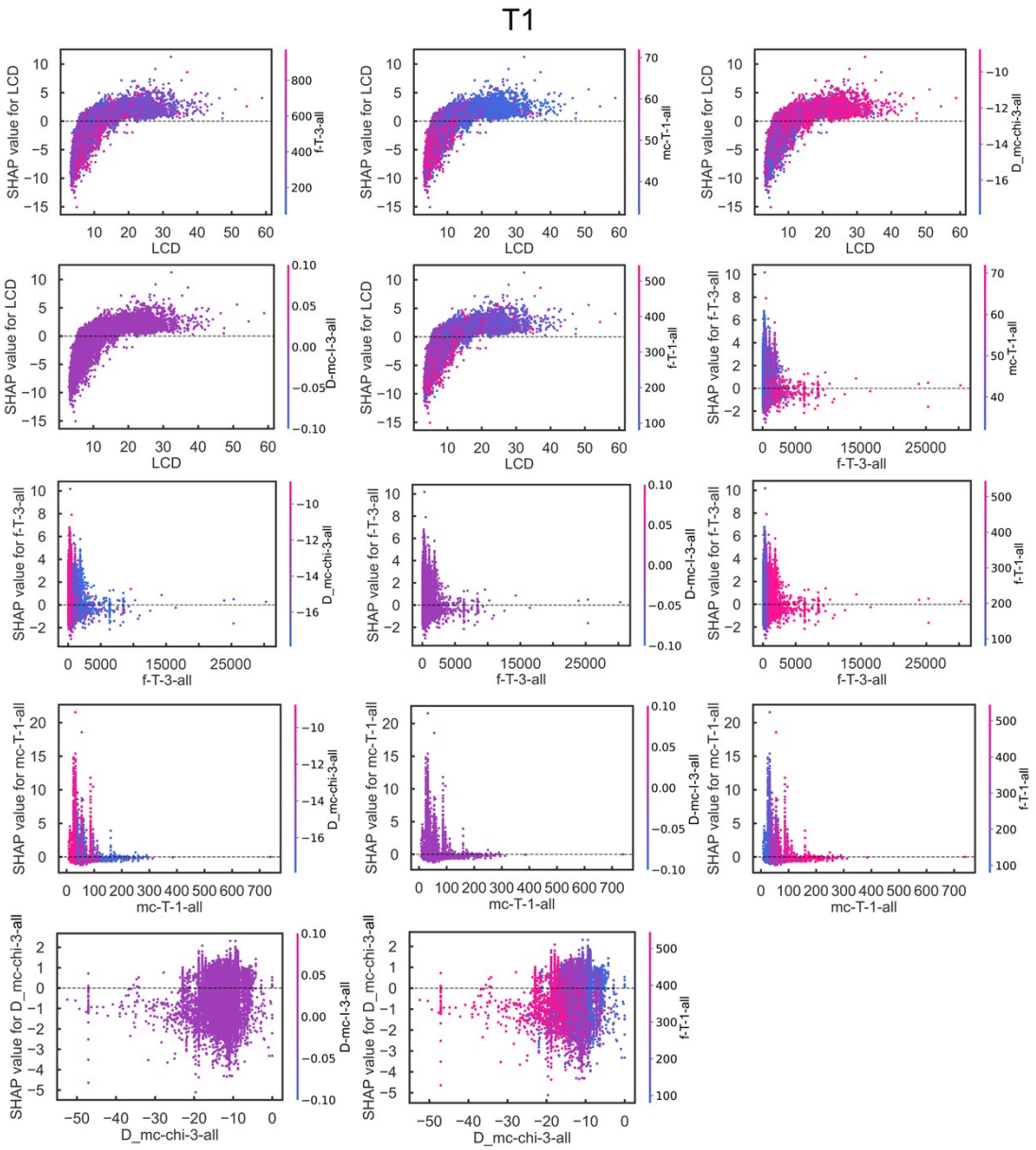

Fig. S4. SHAP dependence plots of T1 for interactions among the top 6 important descriptors.

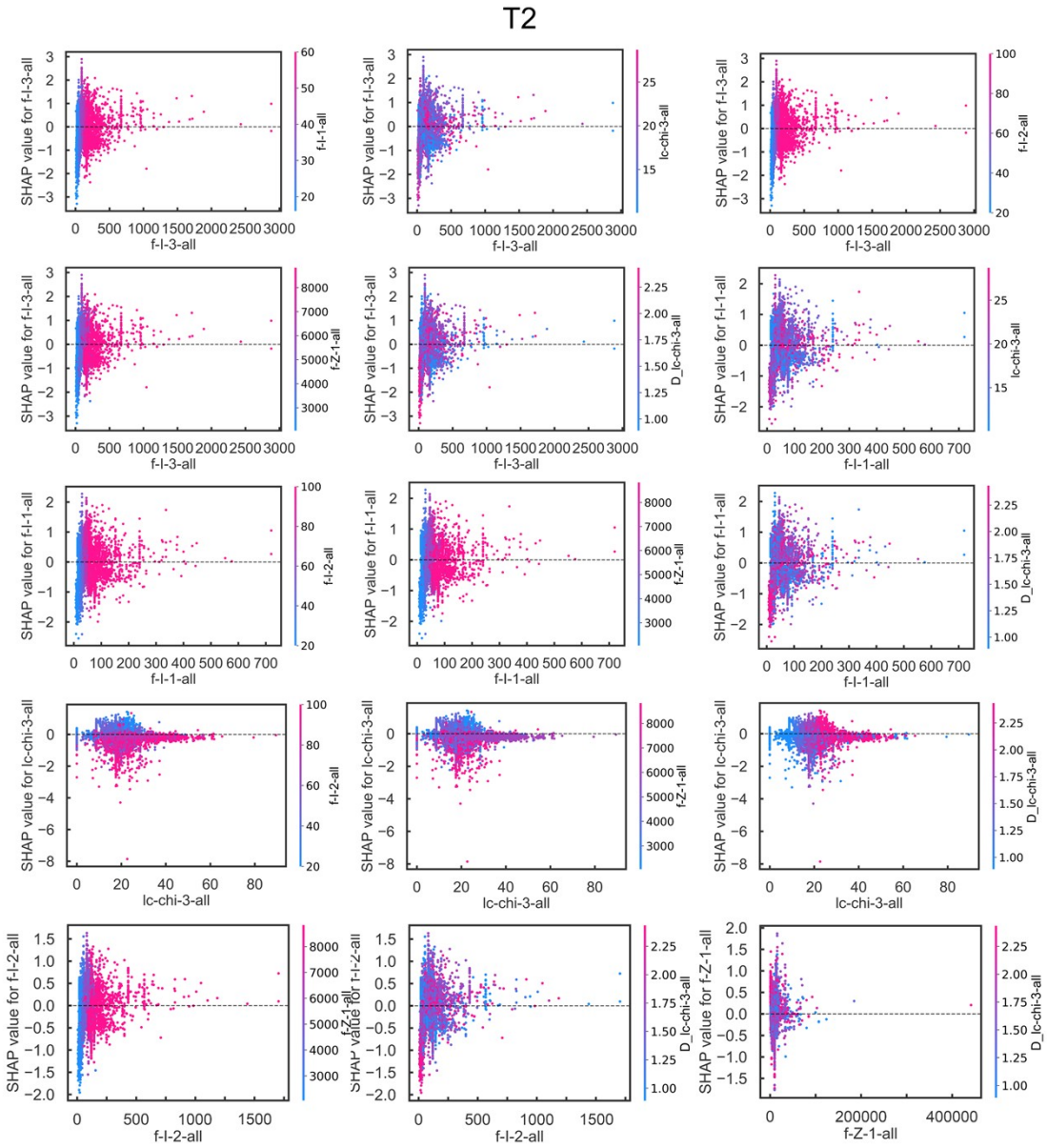

Fig. S5. SHAP dependence plots of T2 for interactions among the top 6 important descriptors.

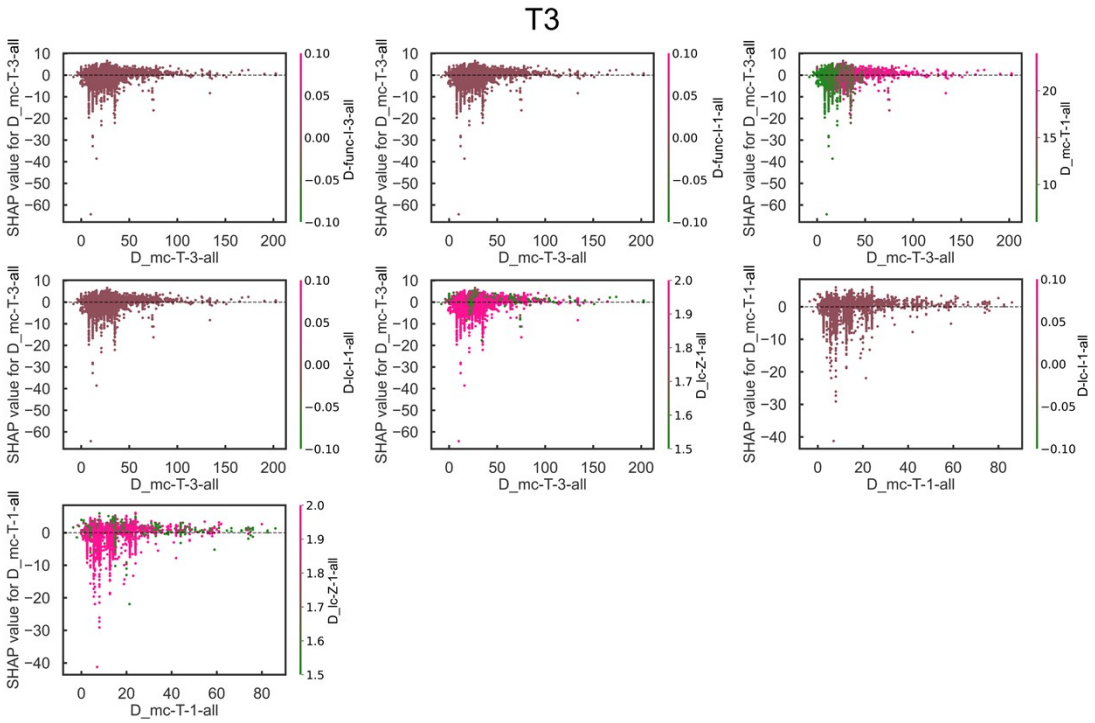

Fig. S6. SHAP dependence plots of T3 for interactions among the top 6 important descriptors.

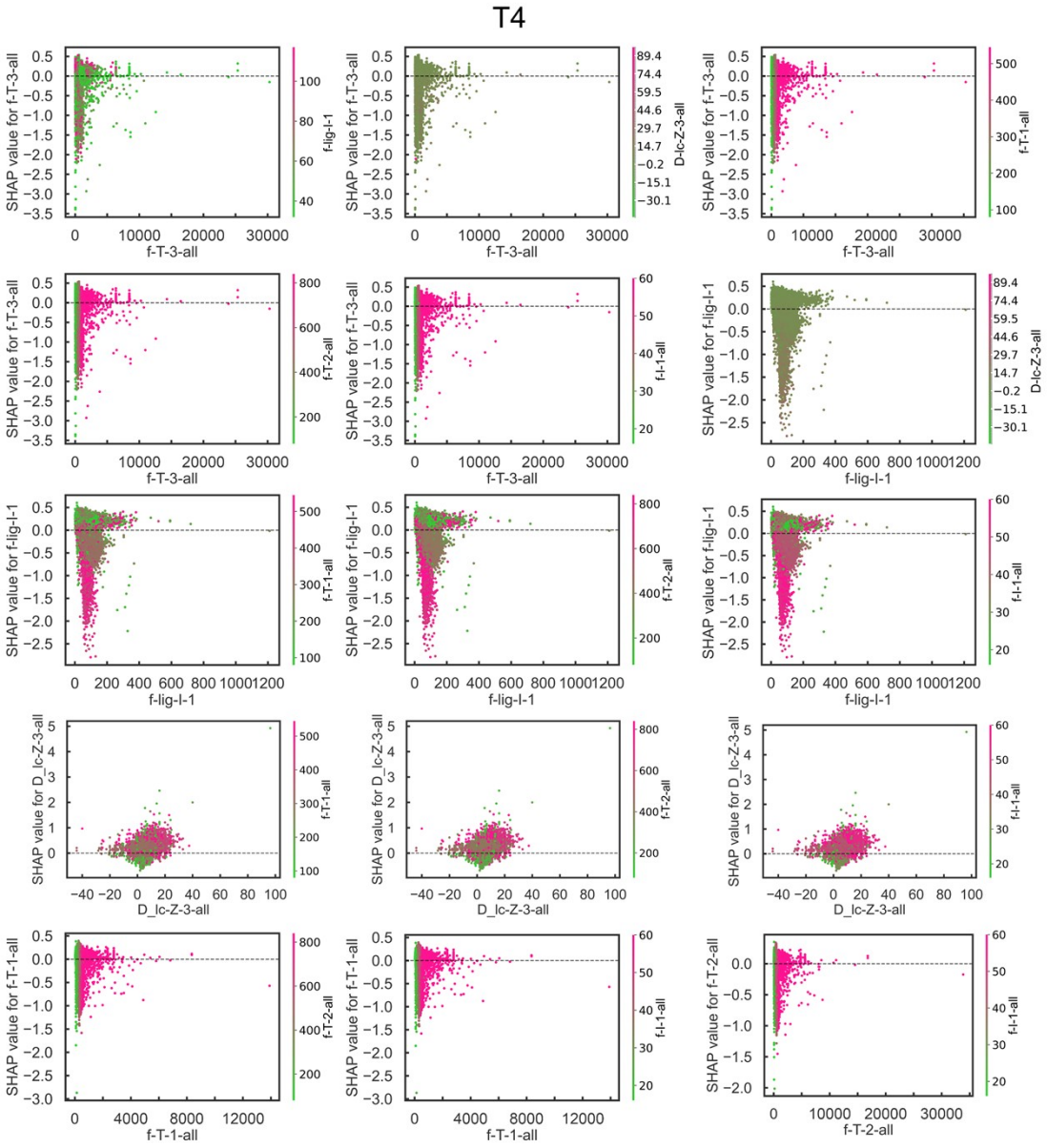

Fig. S7. SHAP dependence plots of T4 for interactions among the top 6 important descriptors.

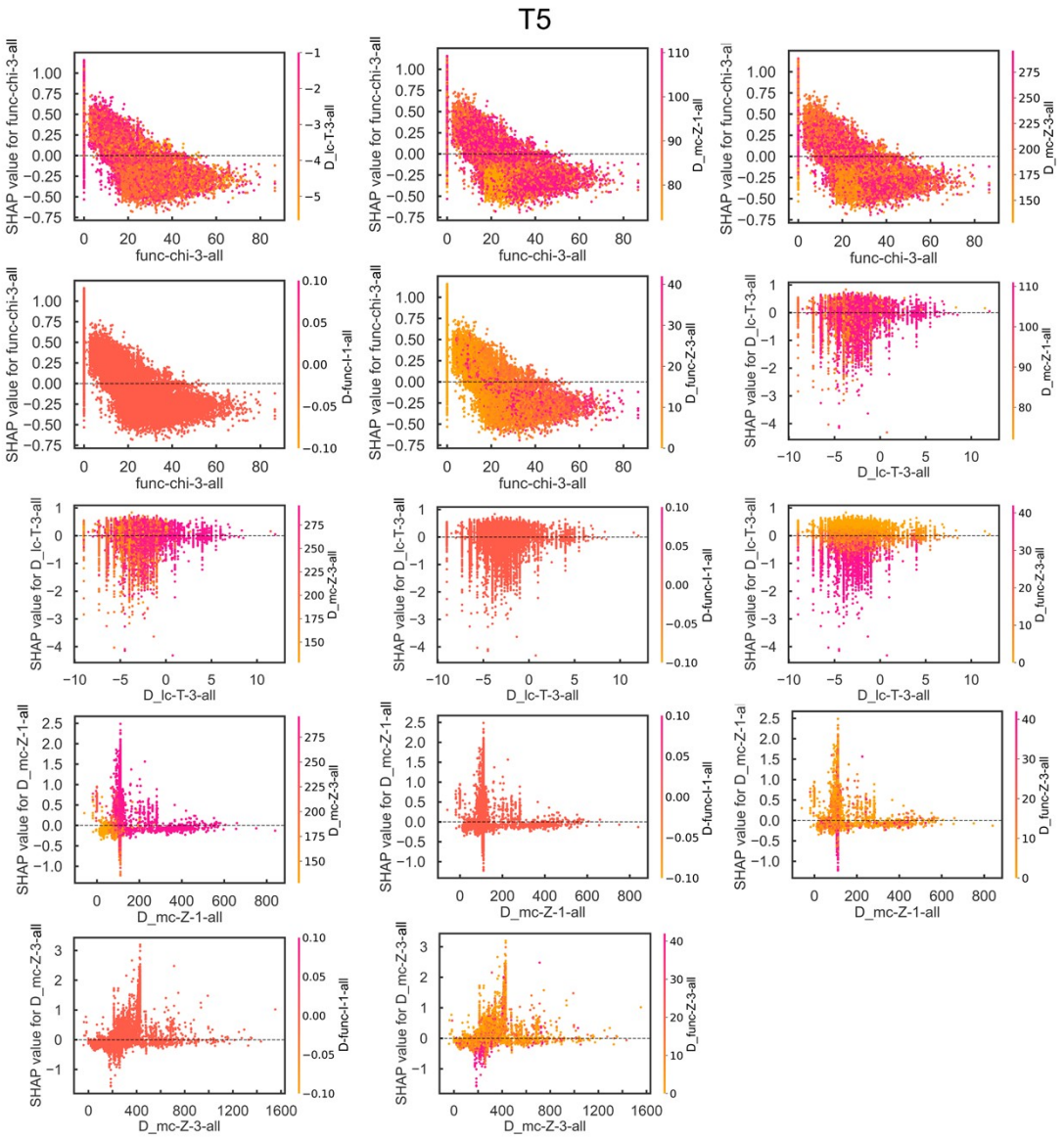

Fig. S8. SHAP dependence plots of T5 for interactions among the top 6 important descriptors.

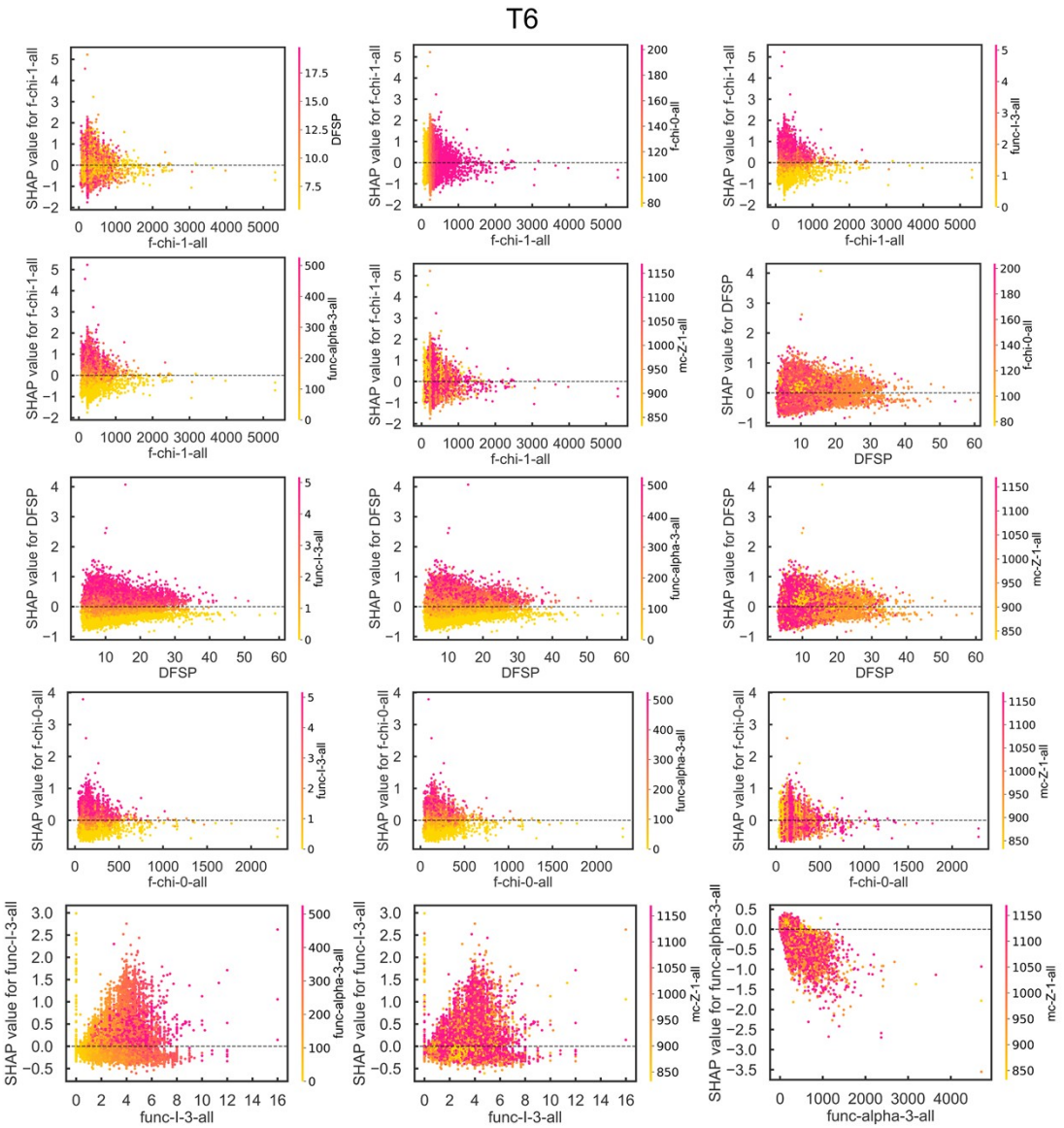

Fig. S9. SHAP dependence plots of T6 for interactions among the top 6 important descriptors.

S5. Feature synergy analysis

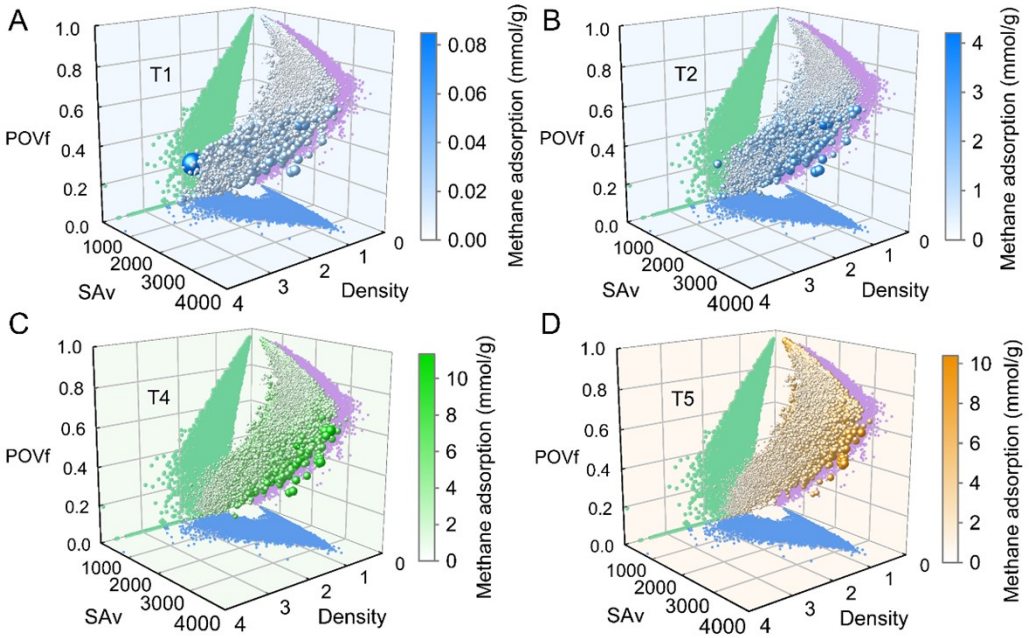

Fig. S10. 3D interaction diagram of three features. (A) POVf, SAv and Density for T1; (B) POVf, SAv and Density for T2; (C) POVf, SAv and Density for T4; (D) POVf, SAv and Density for T5. The size and color intensity of the spheres in the 3D scatter plot correspond to the methane adsorption capacity.

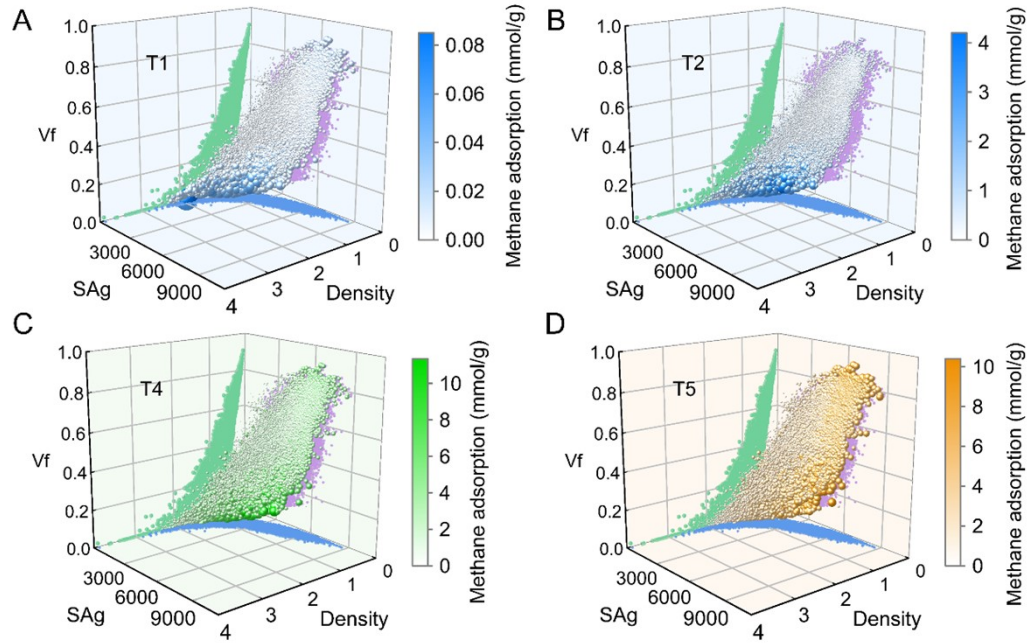

Fig. S11. 3D interaction diagram of three features. (A) Vf, SAg and Density for T1; (B) Vf, SAg and Density for T2; (C) Vf, SAg and Density for T4; (D) Vf, SAg and Density for T5. The size and color intensity of the spheres in the 3D scatter plot correspond to the methane adsorption capacity.

Table S2

MOFs ranking of gravimetric working capacity for PSA1.

MOFs	C_W (g/g)	Density (g/cm^3)	SAg (m^2/g)	POVf	SAv (m^2)	f-lig-S-2	f-lig-I-2	f-lig-I-1	f-lig-chi-3	f-lig-Z-1	f-lig-S-3	topology
m2_o33_o24_xaq	0.929	0.06	6547.78	0.96	398.32	90.97	192.00	120.86	1537.30	3510.86	103.57	xaq
ddmof_15865	0.880	0.06	6786.24	0.95	432.19	64.49	131.43	88.00	1018.68	2701.71	71.67	ptsg
ddmof_16158	0.875	0.06	6654.41	0.95	420.18	64.49	131.43	88.00	1018.68	2701.71	71.67	ptsg
ddmof_16861	0.811	0.08	7712.59	0.93	619.97	216.87	468.00	294.00	3927.98	8034.00	261.01	rtl
m2_o3_lcv	0.787	0.08	6258.08	0.95	488.83	55.88	120.00	76.00	979.50	2112.00	65.54	lcv
m2_o29_nbo	0.783	0.08	6443.34	0.95	518.83	121.24	240.00	144.00	2176.10	4488.00	156.95	nbo
ddmof_21735	0.778	0.08	8013.13	0.94	666.28	85.36	176.00	114.80	1400.79	3393.60	98.43	nou
m3_o29_nbo	0.773	0.08	6406.15	0.95	535.63	121.24	240.00	144.00	2176.10	4488.00	156.95	nbo
m3_o28_unh	0.771	0.08	6288.61	0.95	506.12	90.60	180.00	110.00	1644.95	3504.00	115.17	unh
m2_o28_mou	0.762	0.08	6282.50	0.95	511.27	90.60	180.00	110.00	1644.95	3504.00	115.17	mou

Table S3

MOFs ranking of gravimetric working capacity for PSA2.

MOFs	C_W (g/g)	Density (g/cm^3)	SAg (m^2/g)	POVf	SAv (m^2)	f-lig-S-2	f-lig-I-2	f-lig-I-1	f-lig-chi-3	f-lig-Z-1	f-lig-S-3	topology
SUKYON_clean	0.1438	0.53	5127.16	0.62	2699.55	151.70	324.00	200.00	2761.18	5472.00	190.91	pts
hypotheticalMOF_5074993_0_0_2_23_12_12	0.1391	0.52	4350.75	0.70	2256.03	51.83	136.00	79.33	1009.27	1816.00	60.15	pcu
hypotheticalMOF_16670_0_0_0_22_22_7	0.134	0.59	4307.82	0.64	2534.28	82.17	196.00	112.00	1477.06	2768.00	107.20	pcu
hypotheticalMOF_5073739_0_0_2_23_17_10	0.1291	0.52	3790.21	0.68	1983.09	62.15	161.33	92.67	1208.48	2096.00	74.81	pcu
hypotheticalMOF_5075118_0_0_2_23_18_12	0.1282	0.48	4004.17	0.67	1915.42	60.94	162.67	92.67	1239.48	2048.00	73.92	pcu
UMODEH23_clean	0.1282	0.54	5030.30	0.52	2694.21	131.11	292.00	178.00	2404.79	4896.00	159.82	nbo
hypotheticalMOF_28751_0_0_2_21_21_12	0.1274	0.43	4898.10	0.70	2106.79	51.00	134.67	78.00	985.64	1800.00	59.50	pcu
hypotheticalMOF_5075670_0_0_2_23_23_10	0.1271	0.46	4046.36	0.70	1848.95	75.26	201.33	114.00	1492.84	2464.00	91.82	pcu
m3_o22_o153_f0_pcu	0.1266	0.51	5448.34	0.61	2764.75	101.50	222.67	134.00	1810.49	3618.67	119.09	pcu
hypotheticalMOF_5063673_1_0_2_15_17_10	0.1265	0.53	3924.74	0.65	2098.23	47.80	124.00	72.67	895.45	1696.00	55.97	pcu

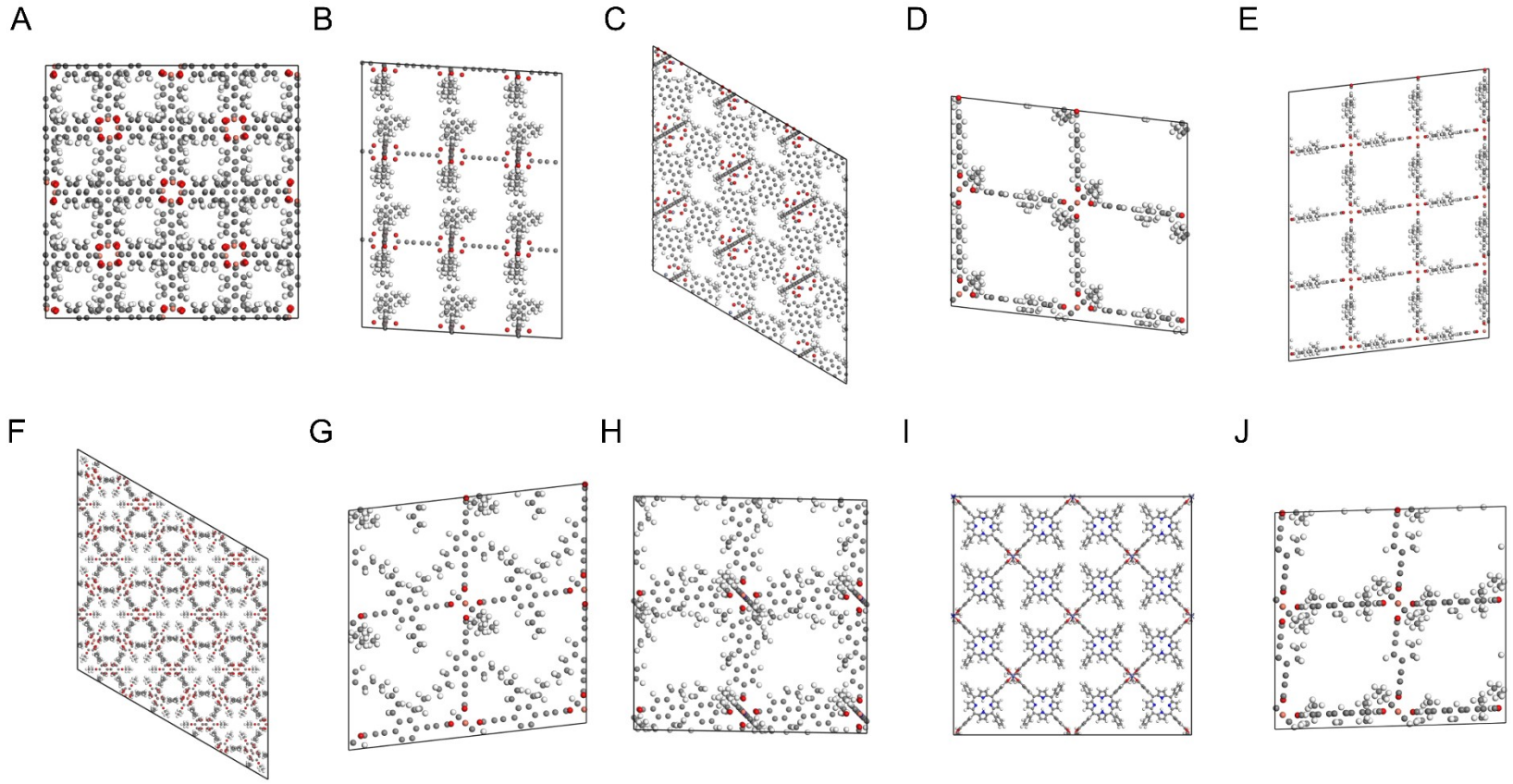

Fig. S12. Structures of top-performing MOFs for PSA2 by gravimetric working capacity: (A) SUKYON_clean; (B) hypotheticalMOF_5074993_0_0_2_23_12_12; (C) hypotheticalMOF_16670_0_0_0_22_22_7; (D) hypotheticalMOF_5073739_0_0_2_23_17_10; (E); (G) hypotheticalMOF_5075118_0_0_2_23_18_12; (F) UMODEH23_clean; (G) hypotheticalMOF_28751_0_0_2_21_21_12; (H) hypotheticalMOF_5075670_0_0_2_23_23_10; (I) m3_o22_o153_f0_pcu; (J)hypotheticalMOF_5063673_1_0_2_15_17_10.

Table S4

MOFs ranking of volumetric working capacity for PSA1.

MOFs	C_W (cm^3/cm^3)	Density (g/cm^3)	SAg (m^2/g)	POVf	SAv (m^2)	f-lig-S-2	f-lig-I-2	f-lig-I-1	f-lig-chi-3	f-lig-Z-1	f-lig-S-3	topology
hypotheticalMOF_5082031_1_0_2_29_13_0	213.45	0.46	4860.10	0.75	2220.85	59.76947	121.33	74.67	1045.85	2264.00	73.53	pcu
Cu2O8-irmof10_A-irmof20_A_No1	210.45	0.49	5323.42	0.76	2588.18	37.336	76.00	49.00	602.36	1590.00	41.15	-
Zn2O8-irmof10_A-irmof20_A_No1	209.50	0.48	5385.69	0.76	2562.29	37.336	76.00	49.00	602.36	1590.00	41.15	-
Zn2O8-irmof10_A-irmof20_A_No31	208.53	0.48	5199.80	0.75	2506.61	37.75565	76.50	49.50	614.34	1615.00	42.08	-
Cu2O8-irmof10_A-irmof8_A_No31	207.55	0.49	5171.93	0.76	2511.52	39.1378	82.00	53.00	683.31	1568.00	45.34	-
Cu2O8-irmof10_A-irmof8_A_No1	207.53	0.47	5377.59	0.76	2542.96	38.2985	81.00	52.00	659.88	1518.00	43.81	-
Zn2O8-irmof10_A-irmof20_A_No21	207.02	0.49	5036.65	0.74	2483.5	38.62	78.00	50.50	628.29	1657.00	43.27	-
m1_o32_pyr	206.62	0.44	4810.67	0.72	2134.5	76.84	162.00	102.00	1353.38	2916.00	92.29	pyr
Cu2O8-irmof10_A-irmof20_A_No19	206.33	0.50	4987.57	0.74	2481.54	39.22	82.00	52.00	639.61	1638.00	44.29	-
hypotheticalMOF_5057404_1_0_1_29_13_0	206.31	0.44	4935.98	0.77	2148.3	59.77	121.33	74.67	1045.85	2264.00	73.53	pcu

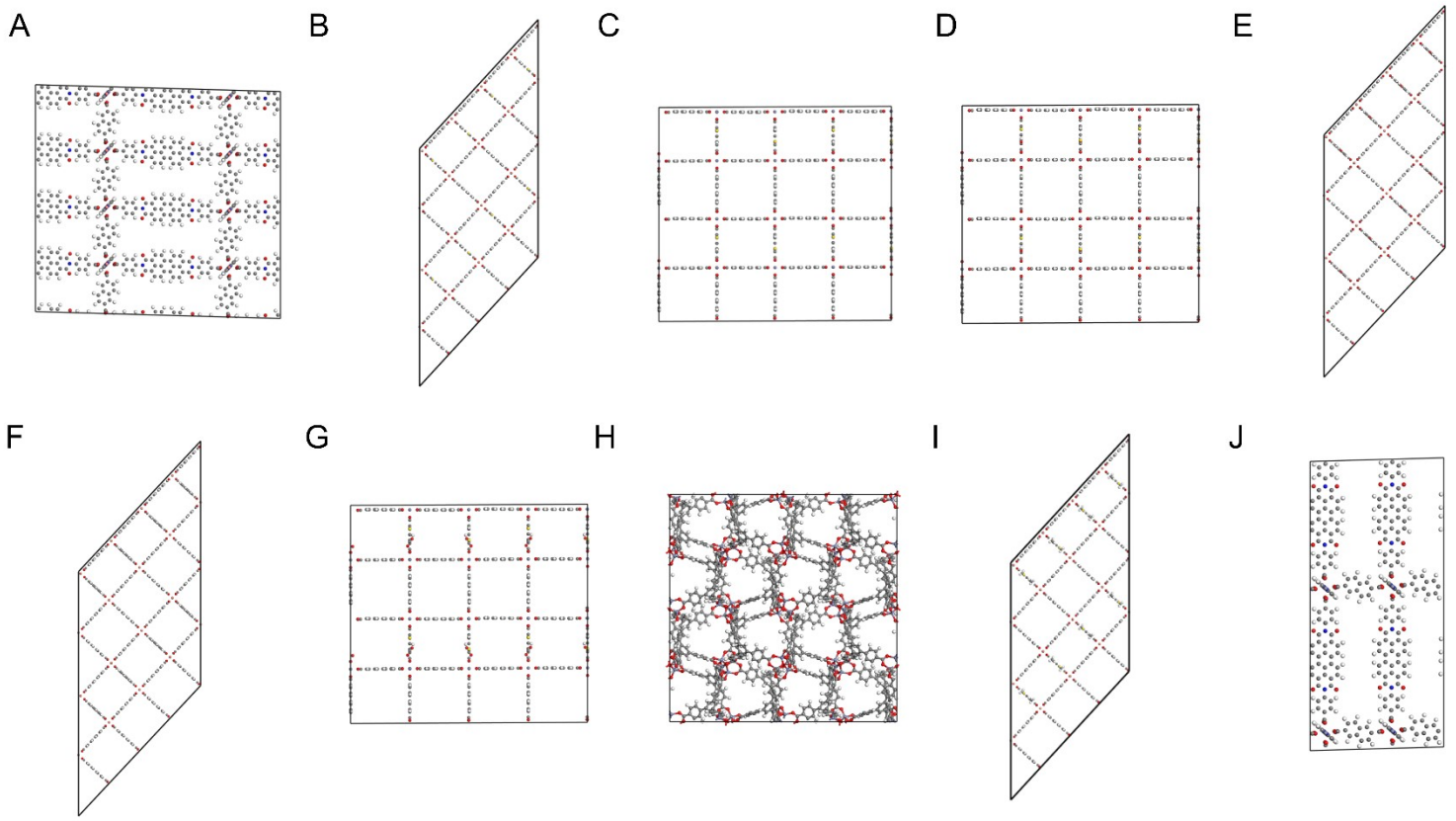

Fig. S13. Structures of top-performing MOFs for PSA1 by volumetric working capacity: (A) hypotheticalMOF_5082031_1_0_2_29_13_0; (B) Cu2O8-irmof10_A-irmof20_A_No1; (C) Zn2O8-irmof10_A-irmof20_A_No1; (D) Zn2O8-irmof10_A-irmof20_A_No31; (E) Cu2O8-irmof10_A-irmof8_A_No31; (F) Cu2O8-irmof10_A-irmof8_A_No1. (G) Zn2O8-irmof10_A-irmof20_A_No21; (H) m1_o32_pyr; (I) Cu2O8-irmof10_A-irmof20_A_No19; (J) hypotheticalMOF_5057404_1_0_1_29_13_0.

Table S5

MOFs ranking of volumetric working capacity for PSA2.

MOFs	C_W (cm^3/cm^3)	Density (g/cm^3)	SAg (m^2/g)	POVf	SAv (m^2)	f-lig-S-2	f-lig-I-2	f-lig-I-1	f-lig-chi-3	f-lig-Z-1	f-lig-S-3	topology
Cu2O8-irmof14_A-irmof6_A_No143	113.07	0.76	2851.81	0.62	2169.94	54.49	99.00	61	899.46	2432	70.52	-
Cu2O8-irmof14_A-irmof6_A_No120	112.32	0.76	2819.21	0.62	2148.13	54.13	98.00	60	879.98	2430	69.75	-
Cu2O8-irmof14_A-irmof8_A_No120	111.34	0.72	2960.70	0.65	2133.19	58.46	111.00	67	968.92	2514	76.18	-
Cu2O8-irmof14_A-irmof20_A_No91	110.68	0.64	3299.35	0.65	2124.09	60.25	130.00	76	1010.43	2298	76.07	-
Cu2O8-irmof14_A-irmof20_A_No107	110.55	0.63	3410.11	0.65	2141.48	60.59	133.00	78	1031.63	2252	76.35	-
hypotheticalMOF_16670_0_0_0_22_22_7	110.06	0.59	4307.82	0.64	2534.28	82.17	196.00	112	1477.06	2768	107.20	pcu
m15_o13_o92_f0_fsc	109.56	0.62	3481.68	0.64	2161.56	75.70	154.00	95	1278.20	2870	89.14	fsc
Cu2O8-irmof14_A-irmof6_A_No121	109.13	0.78	2756.87	0.61	2141.81	54.61	98.00	60	885.17	2478	70.78	-
Cu2O8-irmof14_A-irmof8_A_No152	108.77	0.76	2827.96	0.63	2155.13	59.36	106.00	65	971.70	2900	76.40	-
Cu2O8-irmof8_A-pcn6_A_No4	108.11	0.66	3276.42	0.63	2152.69	49.86	120	70	889.54	1776	62.80	-

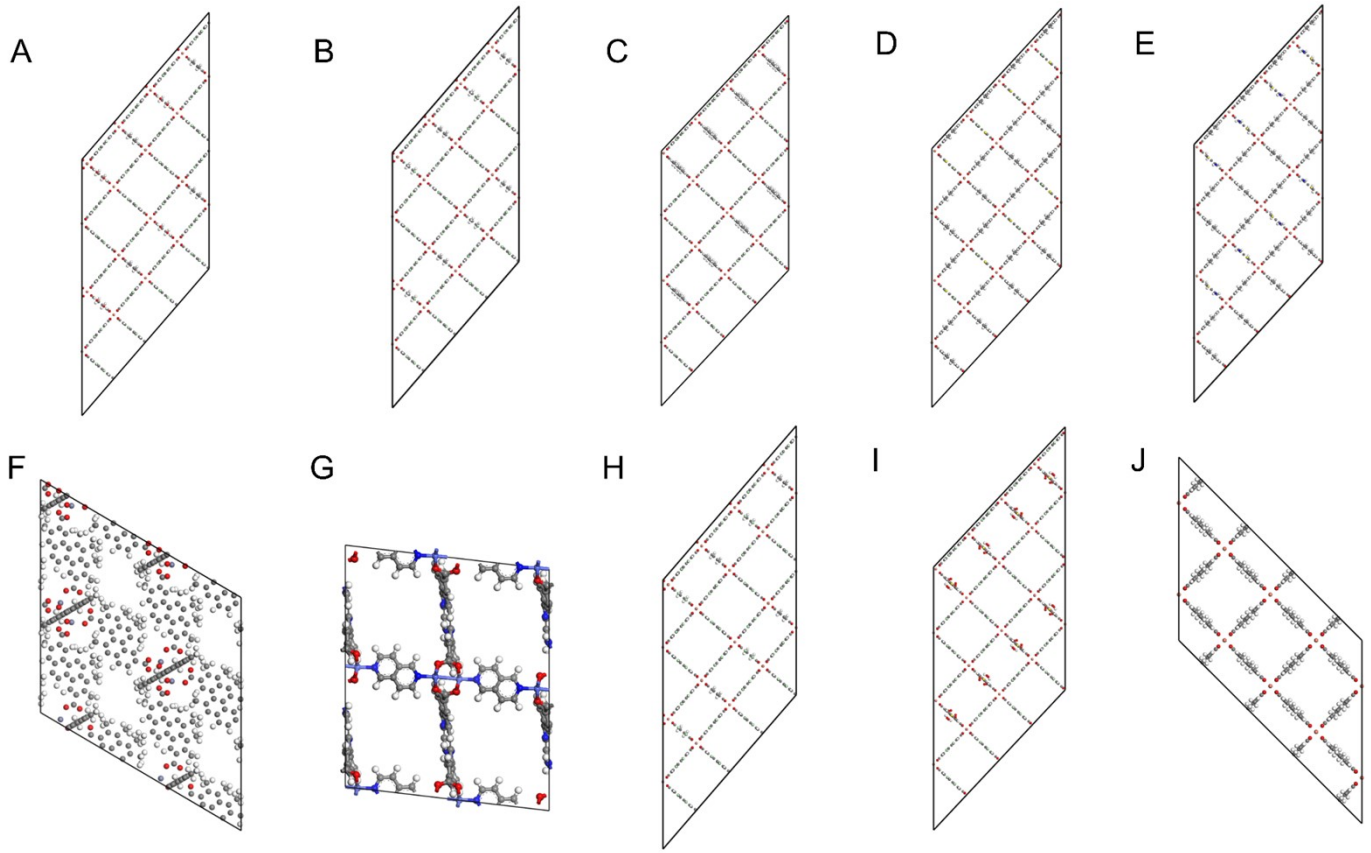

Fig. S14. Structures of top-performing MOFs for PSA2 by volumetric working capacity: (A) Cu2O8-irmof14_A-irmof6_A_No143; (B) Cu2O8-irmof14_A-irmof6_A_No120; (C) Cu2O8-irmof14_A-irmof8_A_No120; (D) Cu2O8-irmof14_A-irmof20_A_No91; (E) Cu2O8-irmof14_A-irmof20_A_No107; (F) hypotheticalMOF_16670_0_0_0_22_22_7; (G) m15_o13_o92_f0_fsc; (H) Cu2O8-irmof14_A-irmof6_A_No121; (I) Cu2O8-irmof14_A-irmof8_A_No152; (J) Cu2O8-irmof8_A-pcn6_A_No4.